
Universiteit
Leiden
The Netherlands

G70.7 + 1.2 - Supernova, nova, or stellar shell?

Jourdain de Muizon, M.; Strom, R.G.; Oort, M.J.A.; Claas, J.J.; Braun, R.

Citation
Jourdain de Muizon, M., Strom, R. G., Oort, M. J. A., Claas, J. J., & Braun, R. (1988). G70.7 + 1.2 - Supernova, nova, or stellar shell? *Astronomy And Astrophysics*, *193*, 248-264. Retrieved from https://hdl.handle.net/1887/7266

Version:	Not Applicable (or Unknown)
License:	Leiden University Non-exclusive license
Downloaded from:	https://hdl.handle.net/1887/7266

Note: To cite this publication please use the final published version (if applicable).

1988A&A...193..248J

Astron. Astrophys. 193, 248–264 (1988)

ASTRONOMY AND ASTROPHYSICS

G 70.7 + 1.2: Supernova, nova, or stellar shell?

M. de Muizon [1,2], R.G. Strom [3], M.J.A. Oort [1], J.J. Claas [4], and R. Braun [5]

[1] Sterrewacht Leiden, Postbus 9513, NL-2300 RA Leiden, The Netherlands
[2] Observatoire de Paris, Section de Meudon, F-92190 Meudon, France
[3] Netherlands Foundation for Radio Astronomy, Postbus 2, NL-7990 AA Dwingeloo, The Netherlands
[4] Laboratory for Space Research, Postbus 9504, NL-2300 RA Leiden, The Netherlands
[5] National Radio Astronomy Observatory, P.O. Box 0, Socorro, NM 87001, USA

Received July 8, accepted August 24, 1987

Summary. We present a set of various data ranging from radio to X-ray wavelengths, including optical spectroscopy and infrared spectrophotometry, of the galactic source G70.7+1.2 whose nature has recently been assessed contradictorily. Our observations definitely confirm the presence of a spherical shock wave expanding in a very dense environment. This shock wave accelerates the relativistic electrons responsible for the shell structure of the radio emission; the fact that we detect weak polarization at 6 cm, but no recombination line emission at 2 cm confirms a dominant synchrotron component. We suggest that G70.7+1.2 could be a young and compact supernova remnant in a high density medium which absorbs part of the non-thermal radio emission, accounting for the turnover in the low frequency spectrum (absorption by thermal electrons). The lower than normal radio luminosity may indicate that the emission is only just turning on, although other possibilities are also likely. The central object, which dominates the near-infrared emission, could be a supergiant star ejecting an envelope. The interaction of ejected matter with the interstellar cloud would lead to the formation of a shock wave propagating in the cloud. G70.7+1.2 might also be interpreted as the remnant of a nova event.

Key words: interstellar medium: bubbles, supernova remnants, H II regions: G70.7+1.2 – infrared radiation – radio continuum – stars: supergiant, novae

1. Introduction

The galactic object G70.7+1.2 is a known source of radio (GC 2002+33), infrared (IRAS 20024+3330) and optical emission (Minkowski, 1948). Optical images of the region around G70.7+1.2, reproduced from the Palomar Observatory Sky Survey (POSS) – O and E – plates, are shown in Fig. 1. The red image of the nebula is brighter and more extended than the blue. It extends over about 1′, while the blue image consists of several patches, 10″ to 15″ in diameter. The blue emission seems to stop where there appears to be dust partially obscuring the red image. A dust lane is particularly obvious on the red image, between the two objects 1 and 2. The nature of G70.7+1.2 has recently been the subject of controversy. Reich et al. (1985) argued that it is a supernova remnant while Green (1986) concluded that it is a compact H II region. Both conclusions were drawn from essentially the same radio data. However, the radio spectrum alone may provide insufficient grounds since, based upon the available radio data, the spectrum of G70.7+1.2 appears rather flat with an average spectral index at the border of the thermal – non thermal discrimination.

We have obtained new observations, ranging from radio to X-ray wavelengths, yielding additional criteria in order to assess the nature of the source. These observations include: i) radio maps at 1515 and 4874 MHz obtained respectively with the VLA and the WSRT, ii) IRAS broad-band photometric data from 12 to 100 μm and IRAS low resolution spectra from 8 to 23 μm, iii) ground-based near infrared photometry and a 3 μm spectrum both obtained at UKIRT (Hawaii), iv) optical spectra between 5100 and 6800 Å at several positions across the nebula, obtained at the INT (La Palma), v) X-ray observations in the 0.2–2.0 keV band obtained with EXOSAT.

Although little is known about the distance to G70.7+1.2, the good definition of its optical structure (Fig. 1) in a direction where extinction in the Galaxy is generally high suggests it is unlikely to be more than a few kiloparsecs (e.g. Green, 1986). Moreover, CO observations made by Bally (private communication) suggest the range 3–5 kpc. Consequently, where it is necessary to assume a distance in our discussion below, we will adopt a value of 3 kpc.

2. Observations and results

2.1. Radio observations

The 20 cm observation was made with the Very Large Array (VLA) in the A-configuration (shortest baseline 0.8 km, longest baseline 36.6 km) on January 28, 1985. It consists of a short 3-min snapshot with a total bandwidth of 100 MHz, split into two 50 MHz channels, centred on 1465 and 1515 MHz. The 1465 MHz channel had to be completely discarded due to excessive interference. The source 3C286 (flux density $S = 14.4$ Jy) was used as primary flux density calibrator.

The initial calibration was carried out at the VLA site. The final reduction was done using the Charlottesville (pre-AIPS) VLA reduction package. After making a map by Fourier trans-

Send offprint requests to: M. de Muizon

© European Southern Observatory • Provided by the NASA Astrophysics Data System

1988A&A...193..248J

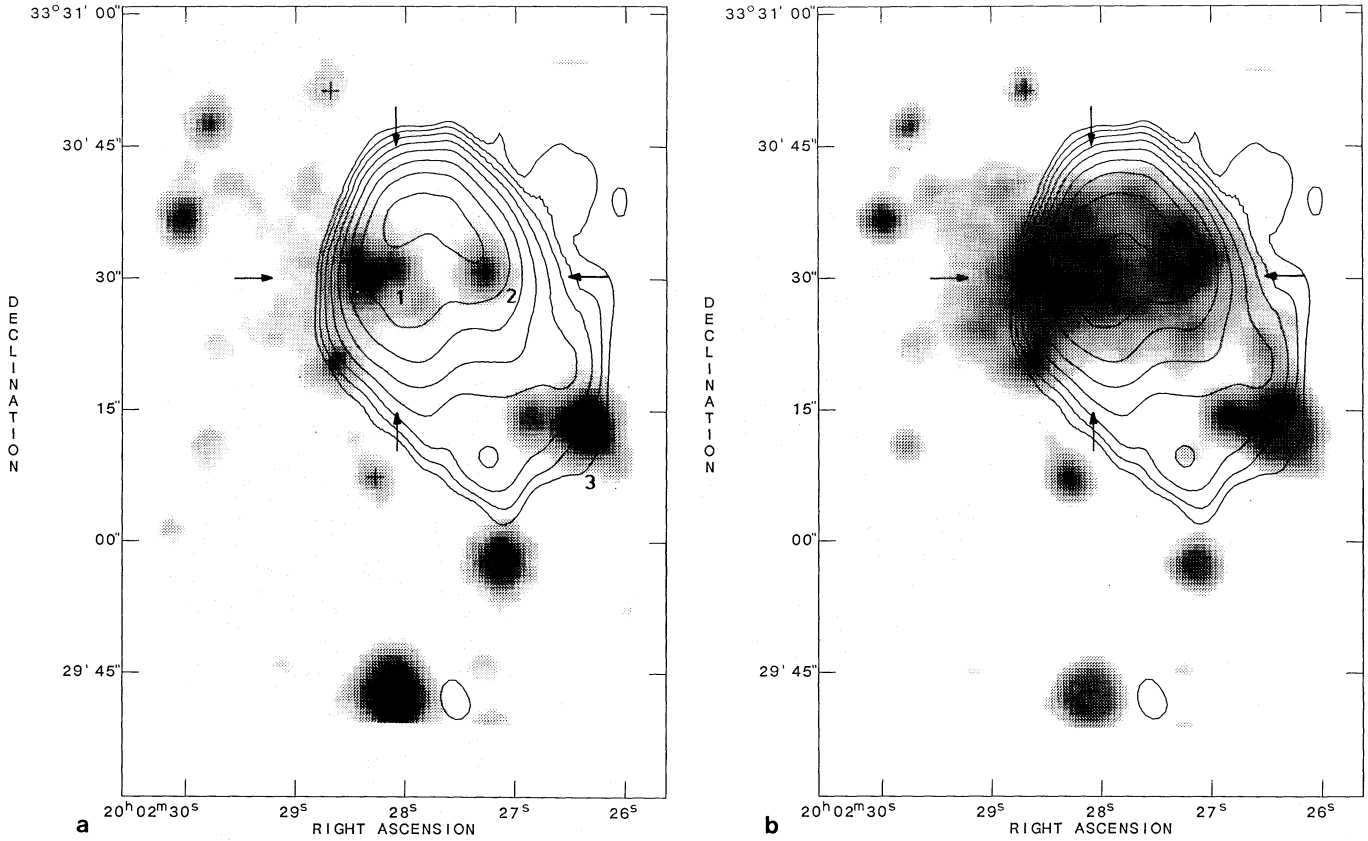

Fig. 1. a Blue image of the region around G 70.7 + 1.2 from the POSS O-plate. Superimposed are contours of the 6 cm WSRT map from Fig. 3. The arrows indicate the ends of the part of the slit through which the optical signal from G 70.7 + 1.2 was recorded. The numbers refer to the objects or stars which are discussed in the text. **b** Same as **a** but on the POSS E-plate (red)

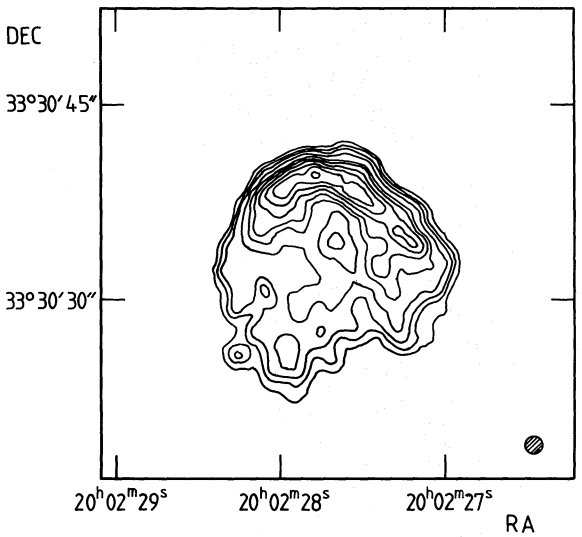

Fig. 2. Cleaned VLA map at 20 cm (1515 MHz) of G 70.7 + 1.2. The beam is 1″. Contours are drawn at 2.5, 3.3, 4.2, 6.0, 8.5, 10, 12, 14, 16, 18, and 20 mJy

formation, clean components were restored with a 1″.4 × 1″.4 gaussian beam. The cleaned 20 cm map (Fig. 2) has an r.m.s. noise of 0.8 mJy. The total integrated flux density at 20 cm is 815 ± 80 mJy. Additional VLA observations were made at 2 cm and 6 cm in the D-configuration to look for recombination line emission. No recombination line was detected with an upper limit for the line to continuum ratio of 1% at 6 cm and 5% at 2 cm.

A 6 cm observation was made with the Westerbork Synthesis Radio Telescope (WSRT) 3-km array, in a 12 hr full synthesis (shortest spacing: 36 m) on November 11, 1985, using the Digital Continuum Backend. The total bandwidth was 80 MHz, separated into eight 10 MHz channels centred on $4839 + 10n$ MHz ($n = 0, 1, \ldots, 7$). The sources 3C147 ($S = 7.6$ Jy) and 3C286 ($S = 7.4$ Jy) were used as primary calibrators. The data quality was improved by using the redundant baselines to determine and eliminate telescope errors (Noordam and de Bruyn, 1982), and by using a self-calibration technique which iteratively removes phase slopes and global gain errors by comparing the visibilities with a CLEAN component model of the source. The dipole configuration available measured the Stokes parameters $I+Q$, $I-Q$, $U+iV$, $U-iV$, the self-calibration only being applied to those combinations where the strong I signal was present.

The quality of the linear polarization (Stokes parameters Q and U) critically depends upon the calibration technique, which is different for Q and U. Q, being measured simultaneously with I, requires good long-term gain stability of the individual dipole channels. During the period in question the gain stability was 1% or better. The quality of U depends upon how well the appropriate dipole combinations can be corrected for cross-talk and non-orthogonality. Indications are that this has also been successful to the 1% level. A map of an observation of the unpolarized source 3C147 done just before G 70.7 + 1.2 shows no polarization greater than 1%.

The data were Fourier transformed with a standard map making routine, using the WSRT Fast Fourier Transform (Brouw, 1971). Grating rings were removed via a clean algorithm

© European Southern Observatory • Provided by the NASA Astrophysics Data System

1988A&A...193..248J

Fig. 3a and b. G 70.7 + 1.2 as observed with the WSRT at 6 cm, the elliptically shaped beam being shown in the lower right-hand corner.

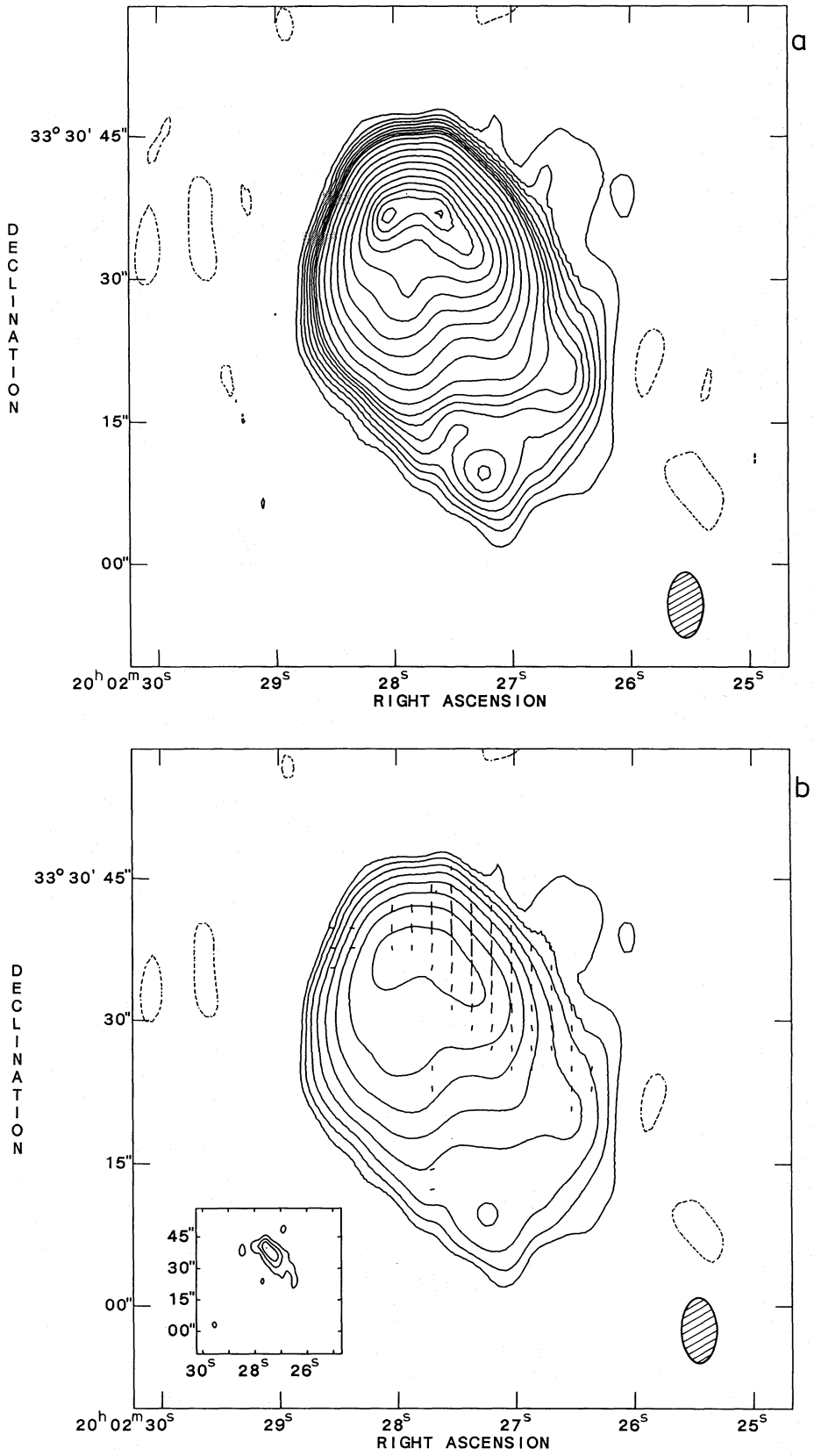

Fig. 3a. The total intensity distribution shown with contours drawn at ±0.55, 1.1, 1.65, 2.3, 3.2, 4.1, 5, 6, 8, 12, 18, 26, 36, 48, 62, 74, 84, 92, and 98% of the peak radio brightness, 57.06 mJy/beam

Fig. 3b. The distribution of linear polarization shown as vectors superimposed upon contours of the total intensity (contour values are ±0.6, 1.2, 2.4, 4.8, 9.6, 19.2, 38.4, 76.8% of the peak value). The longest vector corresponds to a linearly polarized brightness of 1.5 mJy/beam. The linearly polarized brightness distribution is shown in the inset with contours drawn at 25, 50, 75, and 100% of the peak value (the area shown is the same as that of the large plot, with only the seconds and arcsec of the coordinates labelled)

© European Southern Observatory • Provided by the NASA Astrophysics Data System

1988A&A...193..248J

(Högbom, 1974; Clark, 1980). Clean components were restored with a 3".5 × 6".3 gaussian beam. The cleaned map (Fig. 3a) has an r.m.s. noise of 0.25 mJy. The total 6 cm flux density integrated over the whole region is 580 ± 30 mJy. The total 6 cm flux density integrated inside the area delimited by the 3σ-contour in the VLA 20 cm map is 394 ± 12 mJy (this area will be referred to as "the northern shell").

The polarization map (Fig. 3b) apparently shows weak polarization from the northwest rim. Because this is almost exclusively Stokes Q, itself being the result of differencing channels dominated by I, the data have been carefully re-examined. There are two possible types of error, gain and phase, and each will produce a characteristic signature in the resulting map. A gain error is highly unlikely as it will produce something like the I map, with peaks corresponding to the I maxima. A phase error will result in a relative shift of the two maps dominated by I, so the resulting Q map will look like the first derivative of the I map (Q peaks on I gradients). While the Q emission seen does fall on the western gradient, a phase error should produce a comparable Q peak on the (equally steep) eastern gradient. The fact that this is not seen renders such an explanation implausible. The observation of the calibration source 3C147 was also examined for possible phase-shifts between the two I-dominated polarization channels, but nothing significant was found. While a new observation to confirm this result would be desirable, we tentatively conclude that the western rim of G70.7 + 1.2 is partially polarized. Marginal additional support for this conclusion can be drawn from the weak polarization which Reich et al. (1985) suggest may be present in their 6 cm observation. Their degree of polarization, 1.6%, agrees perfectly with our integrated value, although the position angle we obtain (0°) seems to be 45° different from theirs.

2.2. *Infrared observations*

Our attention was originally drawn to G70.7 + 1.2 because of its Infrared Astronomical Satellite (IRAS) Low Resolution Spectrum (LRS) in the 8 to 23 μm range (Fig. 4). We had selected this source from the LRS database together with a sample of a few dozen other sources, because their LRS spectra contained the so-called "unidentified emission features" at 7.7, 8.6, and 11.3 μm. These features, although not precisely identified so far, have been attributed to very small dust grains/large molecules of the Polycyclic Aromatic Hydrocarbon family (Léger and Puget, 1984). Many of the sources selected in our sample also had emission lines from ionized gas such as [Ne II] 12.8 μm and [S III] 18.7 μm in their LRS spectrum and turned out to be compact H II regions (Muizon and Habing, 1985). A few of them, however, had the emission features at 7.7 and 11.3 μm but no sign of [Ne II] or [S III]. The determination of their nature was therefore less straightforward and further observations had to be carried out. IRAS 20024 + 3330 (alias G70.7 + 1.2) was one of them. In the LRS catalogue, the source is classified 8 0. Class 8 contains sources whose LRS spectrum has an emission feature at 11.3 μm; they are in fact mainly compact H II regions and reflection nebulae. The subclass 8 0 contains sources wzose LRS spectrum has the feature at 11.3 μm but no [Ne II] line at 12.8 μm. The good quality (no baseline asymmetry) of the LRS spectrum of IRAS 20024 + 3330, obtained despite the large IRAS beam (several arc minutes) due to the LRS being a slitless spectrometer, allows us to say that the source responsible for this infrared spectrum is less than 20" in diameter.

The source is also listed in the IRAS Point Source Catalogue with a reference position: R.A. (1950) = $20^h02^m26^s.7$, Dec. (1950) = +33°30'25". The survey fluxes are given in Table 1 together with the derived colour temperatures which give an indication of the dust temperature. Inspection of the IRAS skyflux maps shows that the source is not spatially resolved by the IRAS survey instrument.

We have observed the source with UKIRT in September 1985 and June 1986. The strongest signal at 3 μm came from position: R.A. (1950) = $20^h02^m28^s.0$, Dec. (1950) = +33°30'29".6. Magnitudes in J, H, K, L, and L' bands were measured with a 12" beam (Table 1) and a 3.0–3.8 μm CVF spectrum was taken (Fig. 5) in order to search for the 3.3 μm emission feature usually associated with the feature at 11.3 μm. A weak 3.3 μm feature was detected. A 3.2–3.4 μm spectrum was also obtained with a 26" beam. Both the 3 μm continuum and the flux in the 3.3 μm feature are found to be larger in the 26" beam than in the 12", thus showing that the 3.3 μm emission is extended.

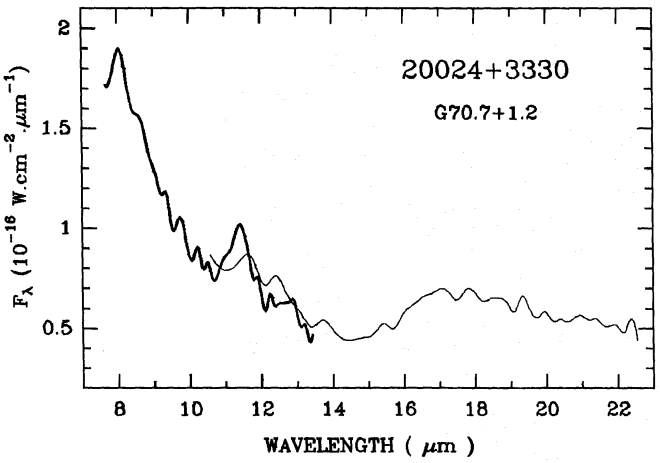

Fig. 4. IRAS low resolution spectrum of G70.7 + 1.2. Thick line: band 1, 7.8–13 μm; thin line: band 2, 10.5–22.5 μm. Inside each band the resolution is ~10 at the blue end and ~40 at the red end

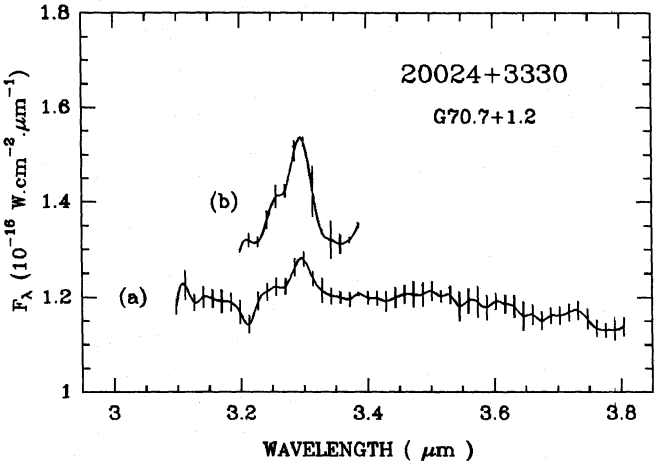

Fig. 5. Near infrared spectrum of G70.7 + 1.2 in the 3 μm region, obtained at UKIRT. (a) With a 12" beam. (b) With a 26" beam

© European Southern Observatory • Provided by the NASA Astrophysics Data System

1988A&A...193..248J

Table 1

a) Near-infrared photometry of G70.7 + 1.2

Band	λ (μm)	Magnitude	F_ν (Jy)
J	1.25	10.2	$1.4\ 10^{-1}$
H	1.65	8.1	$5.9\ 10^{-1}$
K	2.2	6.4	1.76
L	3.45	4.4	5.34
L'	3.82	4.2	5.67

b) IRAS broad-band photometric data

IRAS band	λ (μm)	Inband flux ($W\,m^{-2}$)	PSCAT data (Jy)	Sky flux map[a] (Jy)
Band 1	12	$4.2\ 10^{-12}$	33.3	34.5
Band 2	25	$4.7\ 10^{-12}$	94.8	93.4
Band 3	60	$6.6\ 10^{-12}$	258.3	270.9
Band 4	100	$2.6\ 10^{-12}$	257.5	393.1

[a] Integrated flux density

c) Colour temperatures

T(band 3/band 4)	*T*(band 2/band 3)	*T*(band 1/band 2)
35 K	70 K	177 K

2.3. Optical observations

Optical spectra of G70.7 + 1.2 were obtained in service mode on July 20, 1986 at the Isaac Newton 2.5 m Telescope (La Palma), equipped with the ID Spectrograph and a CCD detector. Two perpendicular scans across the nebula were taken, each scan being about 4'.5 long, and individual spectra measured all along each scan in pixels of 0".66. The positions of the ends of the part of the slit through which the optical signal was recorded are represented in Fig. 1 by the arrows. Along the North–South (hereafter N–S) scan, the spectral coverage was 5100–6610 Å and along the East–West (hereafter E–W) scan, 5100–6800 Å. The spatial resolution was about 1" and the spectral resolution 2000 ($\Delta\lambda \simeq 3$ Å). The total integration time was 600 seconds per scan.

The correction for sky background was determined by selecting the faintest featureless regions along the slit length on both edges of the nebula, and subtracting the average of both these edges from the main signal. In the absence of a standard star measurement, the system response could only be partially calibrated by using a theoretical curve giving the efficiency of the grating and detector used as a function of wavelength.

On the E–W scan, the emission lines [O I] λλ 6300, 6363, [N II] λλ 6548, 6583, Hα and [S II] λλ 6717, 6731 were detected over a distance of about 30". On the N–S scan, the wavelength coverage was limited at the red end to 6610 Å, allowing detection of the [O I], [N II] and Hα lines only, also over a distance of about 30". Individual spectra were averaged over a few arcseconds in order to increase the signal-to-noise ratio, without significantly changing the line strengths and ratios when compared with those in the unsmoothed data. The relative intensities of the various lines, not corrected for extinction, are given in Table 2 for different positions along the scans.

On the E–W scan, two different regions appear clearly: in the western part of the scan over a distance of about 16", the [S II] lines at 6717 and 6731 Å are each comparable in strength to or brighter than Hα; then over about 3", the Hα emission increases suddenly by a factor of about 30, reaching its peak value on this scan at position 19" (see Fig. 6a and b). Then, for the last 13 eastern arcsec of the scan, Hα drops below its peak value by a factor of 4 to 10, although it remains much stronger than all the other lines. Clearly the entire eastern part of the scan is a region of strong Hα emission and the western part is one of weaker Hα emission, with the change in Hα intensity occurring within ~1" at the position of the near infrared source and close to the dust lane. The [S II] lines remain almost equally strong in the two regions. These distributions of the relative line intensities along the scan are shown in Fig. 6a and b and on the spectral map in Fig. 7a; position 0" corresponds to the western end at R.A. = $20^h02^m26^s.5 \pm 0^s.3$ and Dec. = $+33°30'30" \pm 3"$ and position 33" to the eastern end at R.A. = $20^h02^m29^s.2 \pm 0^s.3$ and Dec. = $+33°30'30" \pm 3"$ (these positions are indicated in Fig. 1). A spectrum of the source in the western half of the E–W scan is shown in Fig. 8, and a spectrum in the eastern is shown in Fig. 9.

On the N–S scan, Hα is detected over a distance of about 28". It is not very strong all along the scan except at one position in the middle of the scan where, for a 3" segment, it suddenly becomes very strong reaching values up to 20 times brighter than at its peak value on the E–W scan. Hα is significantly brighter in the northern part than in the southern part of the scan. The [O I] and [N II] lines remain bright all along the scan. The line intensity distributions

© European Southern Observatory • Provided by the NASA Astrophysics Data System

1988A&A...193..248J

Table 2a. Relative line intensities along the East-West scan

Relative position (arcsec)	[O I] 6300	[O I] 6363	[N II] 6548	Hα 6563	[N II] 6584	[S II] 6717	[S II] 6731	σ
West								
[0″–6″]	1140	285	780	2085	1505	1555	2120	50
[6″–8″]	1770	615	725	2960	2660	3090	3890	65
[8″–10″]	2575	625	1175	3950	3285	4380	5870	65
[10″–13″]	2200	1080	1220	5130	2960	4290	5440	60
[13″–16″]	1495	505	210	3320	1805	2905	3805	60
[16″–17″]	2635	445	1125	11325	3075	3930	5845	135
[17″–20″]	2280	925	2735	65555	4935	3505	5200	60
[20″–27″]	1515	410	1520	21465	1780	3085	3955	50
[27″–33″]	200	130	520	5630	540	530	825	50
East								

Table 2b. Relative line intensities along the North-South scan

Relative position (arcsec)	[O I] 6300	[O I] 6363	[N II] 6548	Hα 6563	[N II] 6584	σ
South						
[0″–5″]	375	90	–	1000	150	60
[5″–10″]	1370	335	210	2440	670	50
[10″–12.″5]	3070	1130	895	6625	2580	60
[12.″5–16″]	4495	2175	11680	311135	20345	60
[12.″5–14″]	5095	1810	11510	311710	14005	150
[14″–15″]	9060	6080	34180	991380	57465	150
[15″–16″]	3535	1580	10045	200880	14070	150
[16″ – 24″]	2380	690	1145	7605	2670	35
[24″–30″]	480	75	165	1160	570	60
North						

are shown in Fig. 6c and on the spectral map in Fig. 7b; position 0″ corresponds to the southern end at R.A. = $20^h02^m28^s.1 \pm 0^s.3$ and Dec. = $+33°30'15'' \pm 3''$ and position 30″ to the northern end at R.A. = $20^h02^m28^s.1 \pm 0^s.3$ and Dec. = $+33°30'45'' \pm 3''$. A spectrum of the source in the southern half, at position 10″–12″ of the N–S scan, is shown in Fig. 10.

The optical spectra of G70.7 + 1.2 have strong emission lines but no continuum except at two positions (of spatial extent ≈1.″5), which are very clear in Fig. 7a and b where the continuum has not been subtracted. The first continuum source is located in the middle of the N–S scan (position 13″–16″ in Fig. 7b). It corresponds to an object visible on the POSS blue plate, although it is not clear from there whether it is a star or a nebulosity (object 1 in Fig. 1a). In our optical spectra it appears as a red continuum underlying the emission lines. This continuum is seen to be much brighter on the N–S scan which covered the object totally, than in the E–W scan where it is also detected but much fainter because the slit only covered its edge (position 18″–20″ on the E–W scan). The spectra of this object in both scans correspond to the peak of Hα emission along each scan. A spectrum at the position of this continuum source is shown in Fig. 11 (N–S scan, position 13″–16″). Besides the [O I], [N II] and Hα lines, a number of other emission lines are present (Fig. 11 and Table 4). More strong emission lines are also present in the blue part of this spectrum (Table 4). The spectrum of this continuum source on the E–W scan also exhibits very strong Hα emission, together with strong [O I], [N II], and [S II] lines, and in addition two of the above emission lines, at 6317 Å and 6383 Å; all lines and the continuum are much weaker than on the spectrum in Fig. 11 as noted above. Another star is seen on the E–W scan about 10″ west of object 1 at position 8″–10″. It is in fact located in the middle of the western half, where [S II] > Hα, and is also visible on the POSS blue plate (Star 2 in Fig. 1a). Its spectrum consists of a rather strong and very red continuum, on which are superimposed the emission lines of [O I], [S II] and Hα as they appear in Fig. 8.

2.4. *X-ray observations*

X-ray observations were obtained on 1985 October 27, using the low energy experiment (hereafter LE) on board the European X-ray satellite EXOSAT. The LE experiment is sensitive in the energy range 0.05–2 keV and has an on-axis angular resolution of about 18″. The field of view is about two degrees. The experiment is used in combination with a number of filters; for this observation we used the thin lexan filter only. The total observation time was 30100 s (8.4 h). A search for any detection was carried

© European Southern Observatory • Provided by the NASA Astrophysics Data System

1988A&A...193..248J

Fig. 6a–c. Distribution of the intensities of the strongest optical lines along the scans

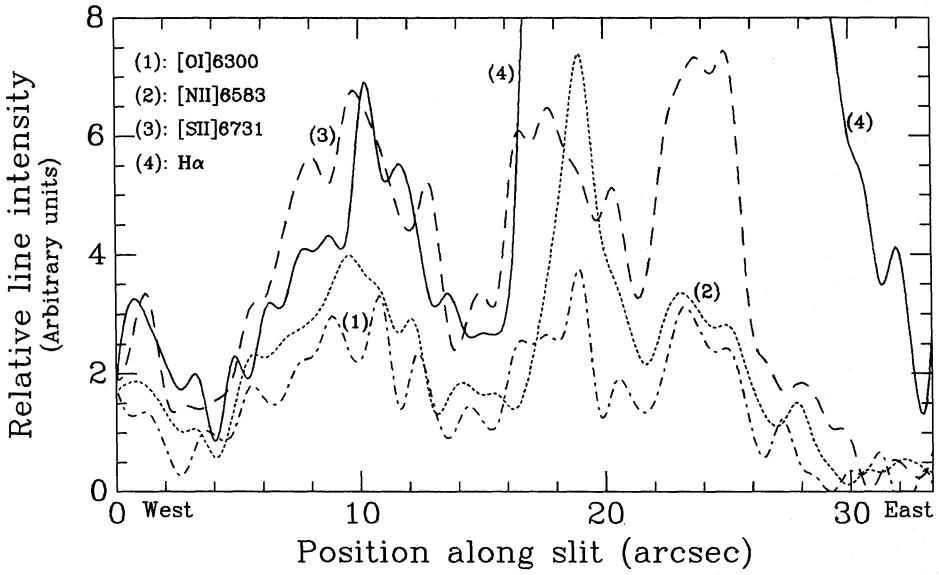

Fig, 6a. Scan E–W, blow-up of the lower part of the diagram

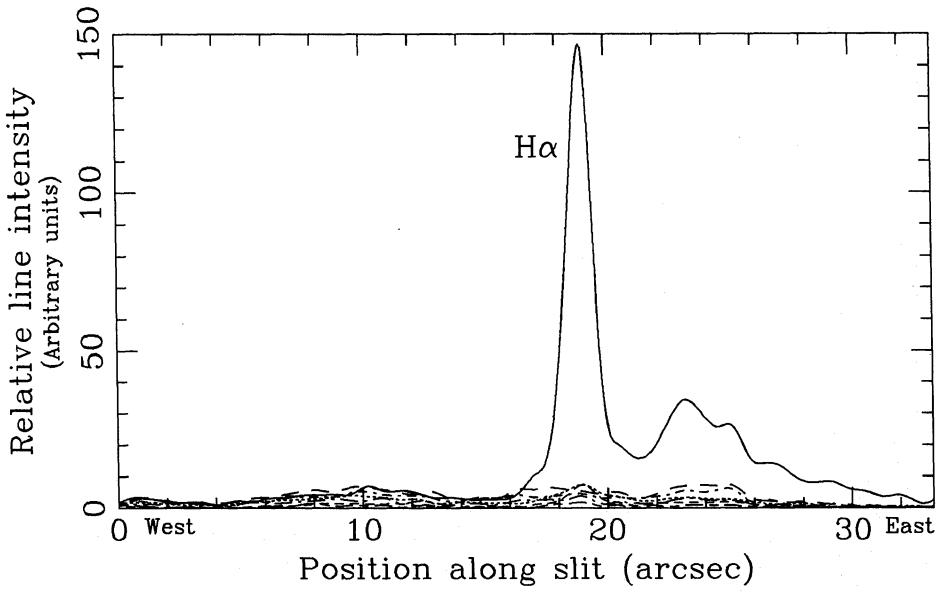

Fig. 6b. Scan E–W, full scale

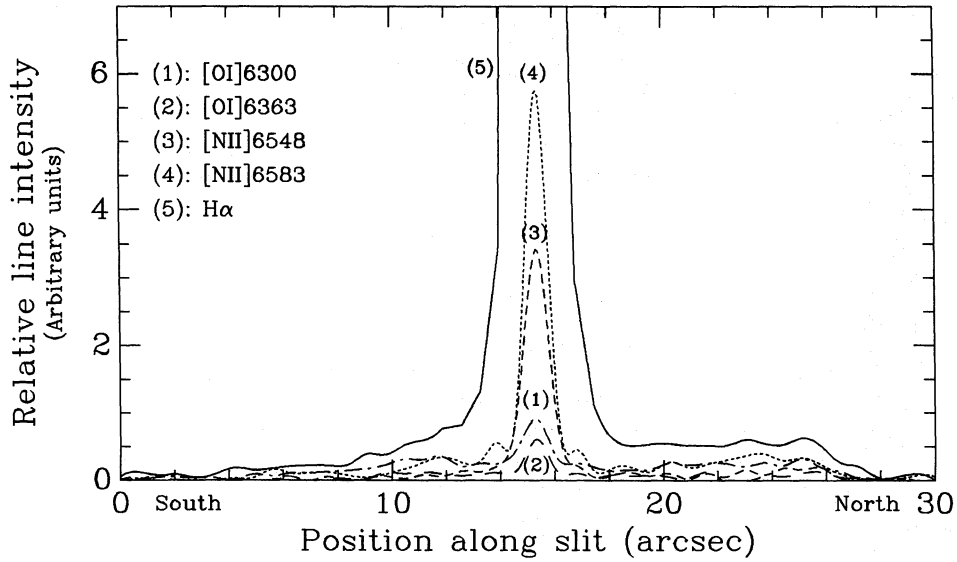

Fig. 6c. Scan N–S, blow-up of the lower part of the diagram

© European Southern Observatory • Provided by the NASA Astrophysics Data System

1988A&A...193..248J

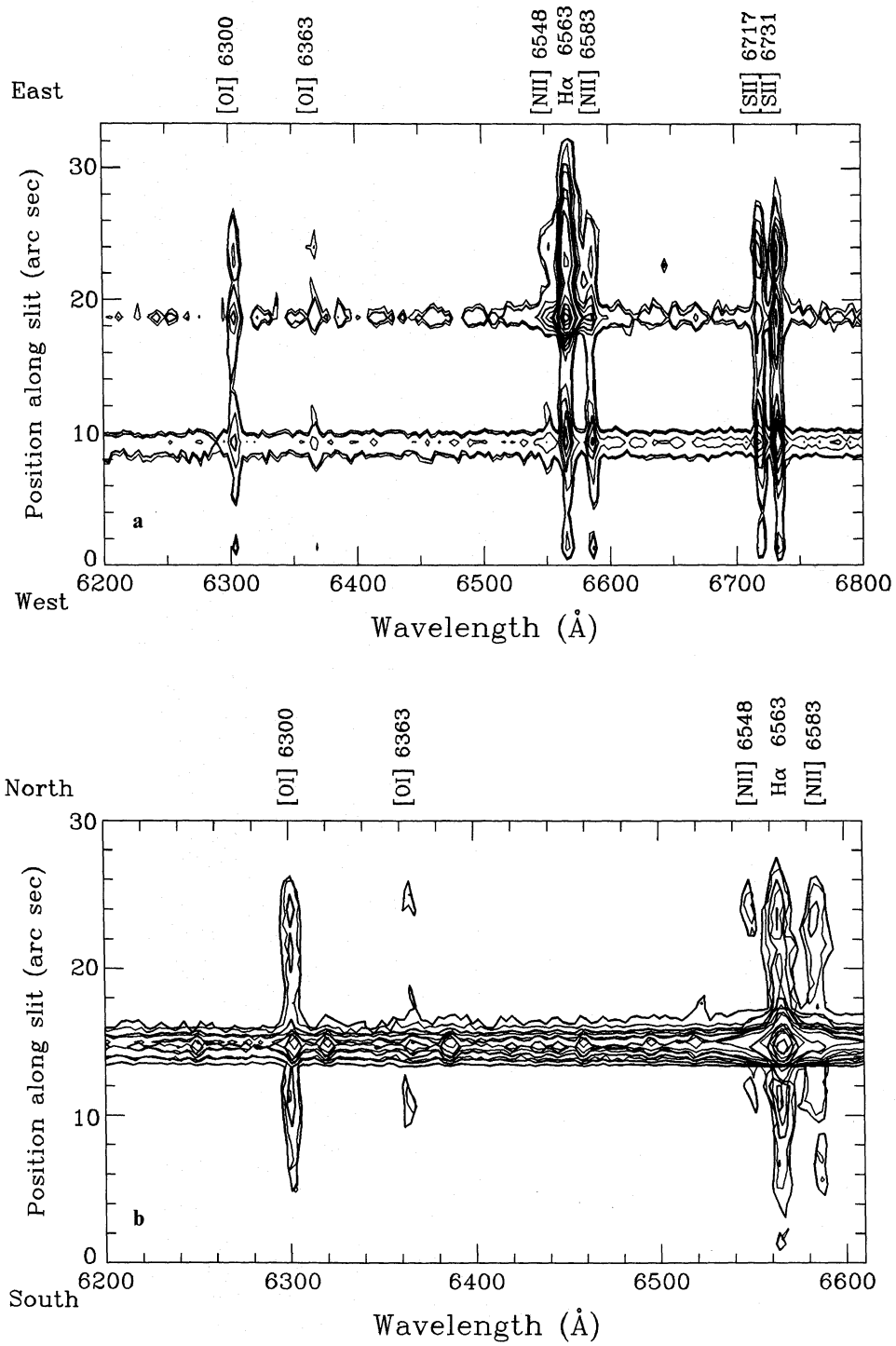

Fig. 7a and b. Contour plots along both spectral scans. Contours are in arbitrary units due to the absence of flux calibration. Continuum sources have not been subtracted and appear clearly on the two maps. Object 1 is seen on scan N–S at position 13″–16″ and partially on scan E–W at position 18″–20″. Object 2 is seen on scan E–W at position 8″–10″. All the [O I], [N II], [S II] and Hα lines are clearly seen, and even the Fe II lines can be seen at several positions on the continuum (scan N–S)

© European Southern Observatory • Provided by the NASA Astrophysics Data System

1988A&A...193..248J

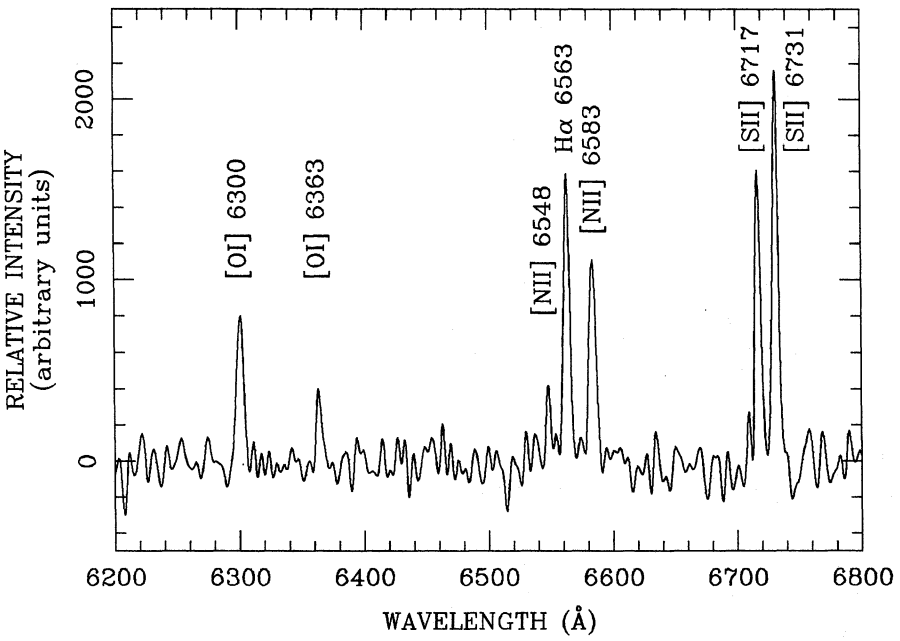

Fig. 8. Spectrum of G70.7 + 1.2 in the western half of the E–W scan at position 6″–8″. The strong [S II] lines (stronger than Hα) and the strong [O I] lines are characteristic of shock-excited gas. In all the spectra (Figs. 8 to 11), the vertical scale, although arbitrary, is the same (same integration time)

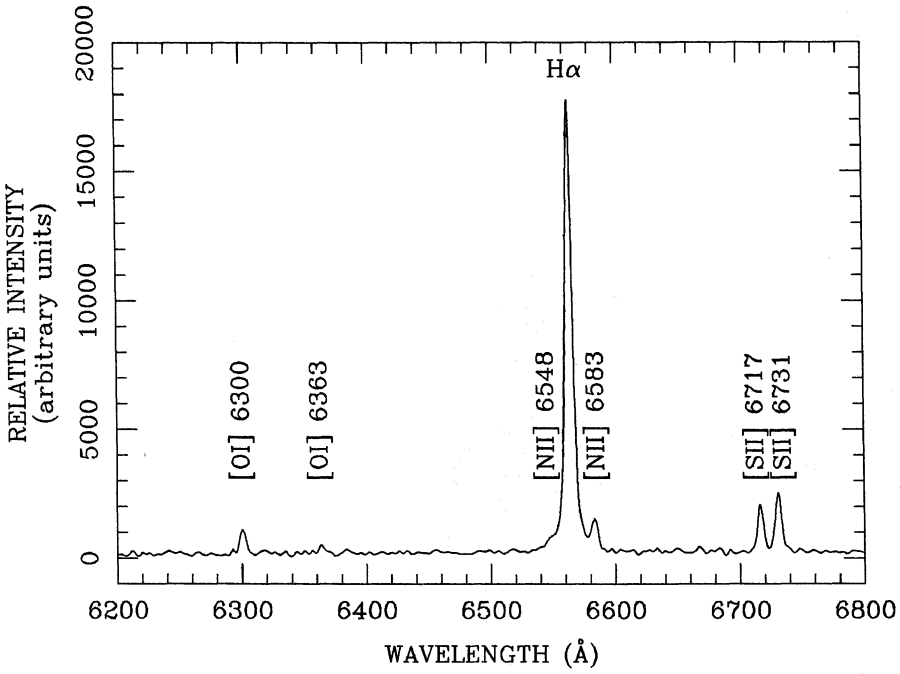

Fig. 9. Spectrum of G70.7 + 1.2 in the eastern half of the E–W scan at position 17″–24″. The [O I] and [S II] lines are still quite bright but strongly dominated by Hα

out by cross-correlating the obtained X-ray image with the point spread function of the LE experiment. In a square region of 34′ × 34′ around the expected position, i.e. R.A. (1950) = $20^h02^m28^s$ and Dec. (1950) = +33°30′35″, no detection was found. The upper limit derived is given in Table 6.

3. Analysis and discussion

3.1. Morphology of G70.7 + 1.2

It is clear from the radio morphology (Figs. 2 and 3) that we see an edge-brightened shell along the northern periphery of the emitting region, with weaker, amorphous emission stretching to the south. A comparison between the optical and radio structures (Fig. 1b) shows that the northern shell runs along the edge of the nebulosity when due account is taken of the elongated 6 cm beam, and this coincidence can be traced along the western edge to the bright star at the southwest (star 3 in Fig. 1a). The resolved radio peak near the southernmost extension also coincides with nebulosity. A weak depression, presumably a dust lane, extends into the bright nebulosity from the northern rim. On the eastern side, nebular emission clearly extends beyond the radio rim.

Looking at the POSS blue image (Fig. 1a), emission is seen only from nebulosity to the east of the dust lane. Indeed, several structural details can be recognised in both the red and blue exposures. The peak in the blue coincides with the strong continuum object seen in the optical spectra (object 1 in Fig. 1a)

© European Southern Observatory • Provided by the NASA Astrophysics Data System

1988A&A...193..248J

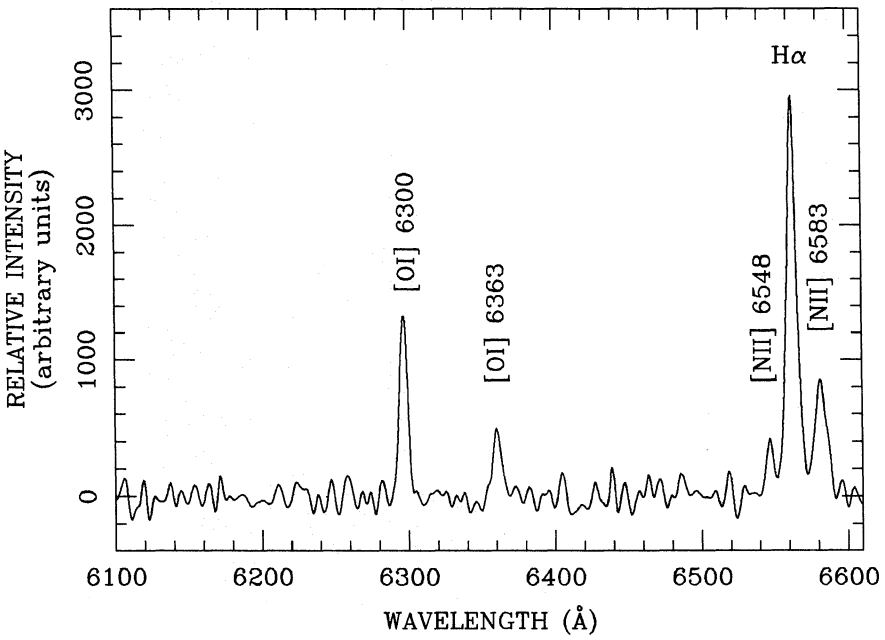

Fig. 10. Spectrum of G70.7 + 1.2 in the southern part of the N–S scan at position 10″–12″. The [O I] and [S II] lines are strong and moderately dominated by Hα

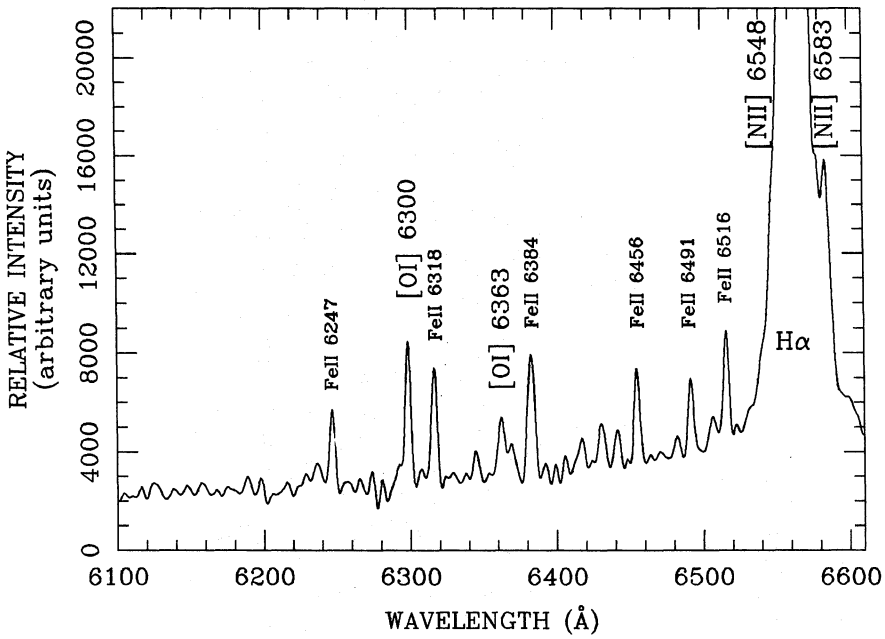

Fig. 11. Spectrum of G70.7 + 1.2 at the position of the continuum source on the N–S scan (position 13″–16″, object 1 in Fig. 1a). In these units, Hα reaches a value of about 10^6. [O I] and [N II] lines are indicated, and so are the strongest of the Fe II lines

which emits so much Hα, and apparently coincides with the near-infrared source. A plausible interpretation of the nebular structure is that the radio shell coincides with optical emission partially hidden by a dust layer, which separates if from nebulosity covering much of the shell and extending beyond its eastern edge. This latter nebular emission must therefore lie between us and the radio shell. We will refer to this geometry in our discussion below.

3.2. Optical line emission: evidence for shock excitation

The most striking result from the optical spectra of G70.7 + 1.2 is the strength of the [O I] λλ 6300, 6363, [N II] λλ 6548, 6584 and [S II] λλ 6717, 6731 lines relative to Hα. The ratio Σ[O I]/Hα reaches 0.8 (Fig. 6a, Table 3), one of the highest values ever observed. Its intrinsic value is likely to be even higher if due account could be taken of the extinction which is certainly quite high in this region. The ratio Σ[S II]/Hα reaches 2.5 which again is one of the highest values ever observed (Table 3).

The high value of the ratio Σ[O I]/Hα rules out the possibility of G70.7 + 1.2 being an H II region only. This is based on the comprehensive grid of model H II regions produced by Stasińska (1982). In this grid, the ratio Σ[O I]/Hα lies in the range 0.003–0.03 (assuming a ratio Hα/Hβ ≈ 3) in the case of one-component density models, and in the range 0.02–0.09 in the case of two-component density models. In the same way, spectroscopic observations of H II regions and planetary nebulae show that the [O I] lines, when detected at all in these objects, are never brighter than 0.1 relative to Hα (see review by McKee and Hollenbach, 1980). The strong [O I] lines in G70.7 + 1.2 are therefore totally incompatible with both models and observations of H II regions.

© European Southern Observatory • Provided by the NASA Astrophysics Data System

1988A&A...193..248J

Table 3a. Line intensity ratios along the East–West scan

Relative position (arcsec)	$\frac{\Sigma[\mathrm{O\,I}]}{\mathrm{H}\alpha}$	$\frac{\Sigma[\mathrm{S\,II}]}{\mathrm{H}\alpha}$	$\frac{\Sigma[\mathrm{N\,II}]}{\mathrm{H}\alpha}$	$\frac{[\mathrm{S\,II}]6717}{[\mathrm{S\,II}]6731}$
West				
[0″–6″]	0.68±0.06	1.76±0.09	1.10±0.07	0.73±0.05
[6″–8″]	0.81±0.06	2.36±0.10	1.14±0.07	0.79±0.03
[8″–10″]	0.81±0.05	2.59±0.08	1.13±0.05	0.75±0.02
[10″–13″]	0.64±0.03	1.90±0.05	0.81±0.03	0.79±0.02
[13″–16″]	0.60±0.05	2.02±0.07	0.61±0.05	0.76±0.03
[16″–17″]	0.27±0.03	0.86±0.04	0.37±0.03	0.67±0.04
[17″–20″]	0.05±0.01	0.13±0.01	0.12±0.01	0.67±0.02
[20″–27″]	0.09±0.01	0.33±0.02	0.15±0.01	0.78±0.06
[27″–33″]	<0.02	0.24±0.03	0.19±0.03	0.65±0.15
East				

Table 3b. Line intensity ratios along the North–South scan

Relative position (arcsec)	$\frac{\Sigma[\mathrm{O\,I}]}{\mathrm{H}\alpha}$	$\frac{\Sigma[\mathrm{N\,II}]}{\mathrm{H}\alpha}$
South		
[0″–5″]	0.46 ±0.15	0.15 ±0.07
[5″–10″]	0.70 ±0.06	0.36 ±0.05
[10″–12.″5]	0.63 ±0.03	0.52 ±0.03
[12.″5–16″]	0.021±0.001	0.103±0.001
[12.″5–14″]	0.022±0.001	0.082±0.001
[14″–15″]	0.015±0.001	0.092±0.001
[15″–16″]	0.025±0.002	0.120±0.002
[16″–24″]	0.40 ±0.02	0.50 ±0.02
[24″–30″]	0.48 ±0.14	0.63 ±0.16
North		

Strong [O I], [N II], and [S II] lines relative to Hα are characteristic of interstellar shocks (McKee and Hollenbach, 1980). This comes from the fact that the post-shock gas has a small fully ionized zone and a large recombination zone, whereas in H II regions and planetary nebulae, the fully ionized zone dominates the recombination zone. Therefore in H II regions, Hα is primarily produced in the fully ionized zone. Behind shocks, Hα is only produced in the recombination zone together with the low-excitation lines.

Theoretical models of interstellar shocks have been computed by Shull and McKee (1979). We have compared the line ratios observed in G70.7 + 1.2 to those obtained from their models, in order to estimate a few physical parameters of the shock. Among the "standard" models, model G from these authors is the most suitable to account for the line ratios observed in G70.7 + 1.2. In this model, for a standard pre-shock density $n_0 = 10\,\mathrm{cm}^{-3}$, standard magnetic field strength $B_0 = 1\,\mu\mathrm{G}$ and "cosmic" metal abundances, the electron post-shock temperature is $T_e = 2.4\ 10^5\,\mathrm{K}$ and the maximum density $n_{max} = 3.16\ 10^3\,\mathrm{cm}^{-3}$. The electron temperature at which $n = n_{max}/2$ is $T_e = 7770\,\mathrm{K}$. The expansion velocity of the shock wave is $V_s = 130\,\mathrm{km\,s}^{-1}$. Model F of Shull and McKee (1979), which is only little different from model G, also fits our observations reasonably well; it gives values of T_e, n_{max} and V_s a fraction smaller than in model G. However, a fit even better than any of the standard models is obtained in model H (non standard, pre-shock density $n_0 = 100\,\mathrm{cm}^{-3}$); it leads to $T_e = 1.8\ 10^5\,\mathrm{K}$, $n_{max} = 7.7\ 10^4\,\mathrm{cm}^{-3}$, $T_e(n_{max}/2) = 3650\,\mathrm{K}$ for $V_s = 100\,\mathrm{km\,s}^{-1}$. The other non-standard models with strong magnetic field or with "depleted" metal abundances, both give line ratios very different from what we observe in G70.7 + 1.2.

The electron density n_e can be inferred from the ratio of the [S II] lines; this density sensitivity of the [S II] lines has been an effective spectral diagnostic in H II regions, planetary nebulae and SNRs for many years. Blair and Kirshner (1985) have calculated the variation of the [S II]6717/[S II]6731 intensity ratio as a function of $(10^4\,\mathrm{K}/T_e)^{0.5}\ n_e[\mathrm{cm}^{-3}]$, using the collisional cross sections of Pradhan (1978) and the new transition probabilities of Mendoza and Zeippen (1982). In G70.7 + 1.2, along the E–W scan, the ratio [S II]6717/[S II]6731 is equal to 0.73±0.06 (Table 3). This leads to $(10^4\,\mathrm{K}/T_e)^{0.5}\ n_e[\mathrm{cm}^{-3}] = 1$ to $1.5\ 10^3$. This (n_e, T_e) dependence is best verified in model H of Shull and McKee (1979), i.e. the model with higher preshock density $n_0 = 100\,\mathrm{cm}^{-3}$, where $T_e = 1.8\ 10^5\,\mathrm{K}$ and $n_{max} = 7.7\,10^4\,\mathrm{cm}^{-3}$. For $T_e = 1.8\ 10^5\,\mathrm{K}$, the above ($n_e$, T_e) relation gives an average density $n_e = 5.2 \pm 1.0\ 10^3\,\mathrm{cm}^{-3}$, a value consistent with the maximum density n_{max}.

We conclude that the relative strength of the [O I], [N II], and [S II] lines to Hα in the western 16″ of the E–W scan and in the southern 12″ of the N–S scan provide strong evidence that we observe shock-excited gas.

In fact the source is rather complex and we also observe some thermal emission from G70.7 + 1.2. The ratio [S II]/Hα is about 2 on an extent of 16″ across the radio shell (scan E–W). Further east, however, the ratio [S II]/Hα drops suddenly within 2″ and it is about 0.2 on an extent of 15″. The variation of the [S II]/Hα ratio with position (Table 3) makes it clear that we see two different regions: non-thermal radiation in the western part of the scan (≈16″) and thermal radiation in the eastern part (≈15″). The two regions are adjacent at least in projection. It is tempting to believe that they are associated because the model providing the best fit to the observed line ratios is the one with a higher pre-shock density ($n_0 = 100\,\mathrm{cm}^{-3}$), a condition which is more likely to happen in the neighbourhood of an H II region/molecular cloud complex rather than in the diffuse interstellar medium.

Although our spectra along the N–S scan unfortunately do not include the [S II] lines, it is still possible to locate the two regions

© European Southern Observatory • Provided by the NASA Astrophysics Data System

1988A&A...193..248J

Table 4. Optical emission lines in the spectra of G70.7 + 1.2 (object 1)[a]

λ_{obs} (±2 Å)	Identification				Other contributor			
	Ion	Multiplet	λ_{lab}					
5159	Fe II	18F	5158.00		Fe II	19F	5158.81	
5168	Fe II	42	5169.03					
5197	Fe II	49	5197.57					
5222	Fe II	19F	5220.06					
5234	Fe II	49	5234.62					
5261	Fe II	19F	5261.61					
5273	Fe II	18F	5273.38					
5315	Fe II	49	5316.61		Fe II	48	5316.78	
5376	Fe II	19F	5376.47					
5412	Fe II	17F	5412.64					
5433	Fe II	18F	5433.15		Fe II	55	5432.98	
5495	Fe II	17F	5495.82					
5527	Fe II	17F	5527.33		Fe II	34F	5527.61	
5533	Fe II	55	5534.86					
5673	Fe II	F	5673.22					
5718	Fe II	39F	5718.2					
5746	Fe II	34F	5746.96					
5754	N II	3F	5754.8					
5991	Fe II	46	5991.38					
6043	Fe II	F	6044.10	$(a^2G–a^2I)$	Fe II	46	6044.53	
6189	Fe II	44F	6188.55					
6247	Fe II	74	6247.56					
6300	O I	1F	6300.23					
6317	Fe II		6318.00	$(z^4D^0–c^4D)$				
6363	O I	1F	6363.81					
6384	Fe II		6383.75	$(z^4D^0–c^4D)$	N IV		6380.77	$(2s^1s–3p^1p^0)$
6417	Fe II	74	6416.90					
6432	Fe II	40	6432.65					
6442	Fe II		6442.97	$(z^4F^0–c^4D)$				
6455	Fe II	74	6456.37		N III		6450–6460	$(3p'^4–3d'^4D^0)$
6482	Fe II	199	6482.28		N I	21	6482.74	
6491	Fe II		6491.28	$(z^4D^0–c^4D)$	N I	21	6491.28	
					N III		6487.81	$(3p'^4–3d'^4D^0)$
6516	Fe II	40	6516.05		Fe II		6517.01	$(z^4D^0–c^4D)$
6563	Hα							
6584	N II	1F	6583.39					

[a] An F after the multiplet number refers to the forbidden lines

(thermal and non-thermal) along this scan. In the first southern 12″ of the scan, the ratio Σ[O I]/Hα and to a smaller extent Σ[N II]/Hα are characteristics of shock-excited gas. In the next 4″, Hα is extremely bright and the line ratios are typical of thermal emission. In the last northern 12″ the ratios are again typical of shock-excited gas.

It is interesting to note that the [O I] and [S II] lines remain very strong all along the scans (Table 2) even in the regions where Hα becomes much brighter so that the line ratios are like those of an H II region. This means that either the Hα emitting region is a high excitation H II region, or that the [O I] and [S II] lines observed in the region of strong Hα are in fact emitted by the shock-excited gas which is superimposed in projection on a low-excitation H II region. We reject the first possibility of a high-excitation H II region because if that was the case we should also see infrared emission lines such as [Ne II] 12.8 μm and [S III] 18.7 μm (or higher ionization states) in the LRS spectrum. These lines being absent, we conclude that the Hα emission in the eastern half of the E–W scan comes from a low-excitation H II region located on the line-of-sight and also to the east of the region of shock-excited gas. This H II region is clearly seen on the POSS images (Fig. 1) where it appears as diffuse extended emission to the east of the radio shell. Variations in the wavelength of the peak of the various optical lines indicate velocities in the 100–200 km s^{-1} range.

It is common to identify as a supernova remnant a source of optical emission, with strong [S II]/Hα line intensity ratio ([S II]/Hα ≧ 0.7), and coinciding with radio emission. This criterion has been used extensively (Mathewson and Clarke, 1973; review by Raymond, 1984, and references therein; Longmore et al., 1977; Danziger et al., 1979; Dennefeld and Kunth, 1981; Blair and Kirschner, 1985; Fesen et al., 1985). However, it is not obvious that the SNR diagnostic criterion, although amply satisfied, can be applied to G70.7 + 1.2. Several results from the observations presented in this paper suggest also some other possibilities. These

© European Southern Observatory • Provided by the NASA Astrophysics Data System

1988A&A...193..248J

will be summarized in Sect. 4. One of them arises directly from the optical spectra. The object emitting the red continuum, very strong Hα and several other emission lines, in addition to those of [O I], [N II], and [S II], if associated with the radio source, is not what is commonly found in supernova remnants. The lines detected at the position of object 1 are listed in Table 4. Most of them can be identified as forbidden or permitted lines due to quadrupole transitions of Fe II. The identifications have been made using the list of lines observed in η Carinae and in Nova RR Telescopii (Thackeray, 1967, 1977), and the list of lines detected in the red spectrum of Wolf-Rayet stars (Vreux et al., 1983). It turns out that all the Fe II lines detected towards object 1 in G70.7 + 1.2 are among the brightest of those reported by Thackeray in η Car and Nova RR Tel. The presence of all these lines suggests that object 1 could be a nova-like object, since it has most of the lines typical of the so-called "η Car stage" of slow novae. These objects have a nucleus subject to strong irregular outbursts; however an "η Car event" has been thought to correspond to the very early stages of a massive star (Gratton, 1963). Still based on its optical spectra, object 1 in G70.7 + 1.2 could be a B[*e*] supergiant star falling in the category of "Luminous Blue Variables" or LBV's (Stahl et al., 1985). Since there seems to be evidence of N II and N III in the spectrum, it is possible that this supergiant will become a regular Population 1 Wolf-Rayet star (Chiosi and Maeder, 1986).

3.3. *The radio shell emission*

The radio emission from G70.7 + 1.2 has a shell morphology, and the detection of polarization at 6 cm indicates the presence of synchrotron emission. This is confirmed by the non-detection of recombination line emission at 2 cm; based on experience with other sources it should have been detected if G70.7 + 1.2 was an H II region. Consequently most of the 2 cm emission must be non-thermal in nature. As evidenced by the optical spectroscopy, most of the radio shell coincides with the region of shock-excited gas; thus we conclude that the shell structure of the radio emission is due to relativistic electrons accelerated by shock waves. G70.7 + 1.2 has been observed, at times serendipitously, by several authors. The available radio data are summarized in Table 5, and plotted in Fig. 12. From the available data it is difficult to determine precisely a spectral index which fits the data over the whole radio range. A best fit yields a value for $\alpha \approx 0.4$ ($S_\nu \propto \nu^{-\alpha}$), but in fact at frequencies higher than 1 GHz the spectral index is $\alpha \approx 0.55$ (Reich et al., 1985), while the radio spectrum is much flatter at low frequencies (below 1 GHz).

The 6–20 cm spectral index derived from our observations has been determined by summing the pixel intensities in the VLA and WSRT maps within the area circumscribed by the 3σ-contour in the VLA map (after having degraded the spatial resolution of the VLA map to that of the WSRT map). This was done in order to avoid possible contamination from the neighbouring H II region in the WSRT map. Note that the greater sensivity to extended emission in the WSRT map will, if anything, cause the 6 cm flux density to be overestimated and the spectrum to appear too flat. The resulting spectral index is: $\alpha_{6\,\mathrm{cm}}^{20\,\mathrm{cm}} = 0.62 \pm 0.11$ in agreement with Reich et al. (1985).

However, the determination of the overall spectrum from these measurements is difficult because the radio emission may be confused by a neighbouring H II region; therefore observations obtained with a large beam are not very accurate and this is reflected in the scatter in the data points (Fig. 12).

But whatever the exact shape, one feature cannot be ignored if we are to maintain that a substantial non-thermal component is present. That is the low frequency turnover indicated by the 151 MHz flux density. We believe that this can be quite naturally explained as due to free-free absorption in the H II region which, as we have argued above, must lie in front of the non-thermal shell.

Free-free absorption will produce a cutoff in the spectrum below a frequency of about (Scheuer and Williams, 1968),

$$f_0 \approx 0.6\, n_0\, l^{1/2}\, T_e^{-3/4}\ \mathrm{MHz}$$

where n_0 is the electron density (in cm^{-3}), l is the depth of ionised material (in pc) and T_e is the gas temperature (in 10^4 K). The

Table 5. Radio continuum spectrum of G70.7 + 1.2

Freq. (MHz)	Flux density (Jy)	Beamsize (arcmin)	Ref.
151	0.78 ± 0.15	2 × 4	Green (1986)
408	0.94 ± 0.09	1.5 × 2.6	Green (1985, 1986)
408	1.43 ± 0.14 [a]	4 × 10	Colla et al. (1970)
610	1.24 ± 0.13 [b]	1.0 × 1.8	Israel (1976)
1407	0.80 ± 0.06	0.4 × 0.8	Green (1985)
1415	0.88 ± 0.09	0.4 × 0.8	Israel (1976)
1422	1.1 ± 0.1	2.5 × 4.6	Read, see Green (1986)
1515	0.81 ± 0.08 [c]	0.02	This paper
2695	0.77 ± 0.08	4.3	Reich et al. (1984)
4750	0.58 ± 0.04 [d]	2.4	Reich et al. (1985)
4874	0.40 ± 0.01 [c]	0.06 × 0.11	This paper
4874	0.58 ± 0.03	0.06 × 0.11	This paper ("extended")
22364	0.24 ± 0.02 [d]	0.7	Reich et al. (1985)

[a] Reduced to flux density scale from Baars et al. (1977)
[b] Redetermined and reduced to flux density scale from Baars et al. (1977)
[c] Northern shell only
[d] Estimated from Fig. 3 of Reich et al. (1985)

© European Southern Observatory • Provided by the NASA Astrophysics Data System

1988A&A...193..248J

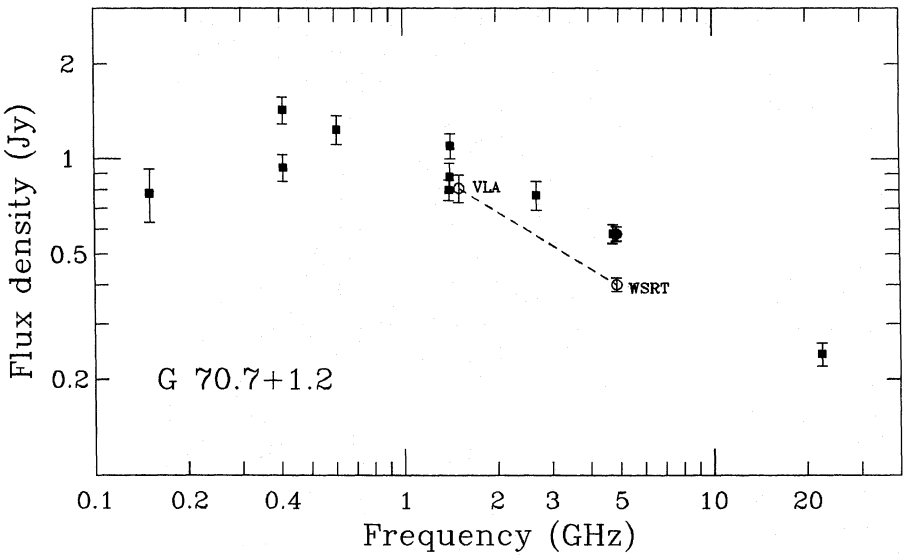

Fig. 12. The radio spectrum of G70.7 + 1.2. All data points are from Table 5. It is apparent from Table 5 that some of the measurements were obtained with a large beam and therefore may be affected by confusion. Filled squares are previously published data; circles are data presented in this paper, open circles referring to the northern shell (see text)

nebulosity (Fig. 1) is about the same size as the radio shell, so we will assume a diameter (and hence depth) of 15″, giving a distance dependent size of 0.07 pc/kpc. The cutoff frequency is about 300 MHz (Fig. 12), so for a distance of d kpc we obtain,

$$n_0 \approx 1760\, T_e^{3/4}\, d^{-1/2}\,\mathrm{cm}^{-3}. \quad (1)$$

For $d = 3$ kpc and $T_e \approx 10^4$ K, a density of 1000 cm^{-3} is indicated, a value also similar to that found above for the shocked gas. This is not surprising if the shell and H II region are in close proximity, and it indicates that some of the free-free absorption may take place in the shell itself.

We must ask ourselves whether such a high density is plausible. Will it lead to too high a mass, or excessive thermal radio emission? The mass implied by the density obtained above is,

$$M = 7.6\ 10^{-3}\, d^{5/2}\, T_e^{3/4}\, M_\odot$$

or only 0.1 $M_\odot$ for $d = 3$ kpc and $T_e = 10^4$ K, hardly an unreasonable value. To calculate the amount of thermal emission, we must first determine the optical depth,

$$\tau = 0.4\, T_e^{-3/2} f^{-2} \int n_0^2\, dl. \quad (2)$$

At a wavelength of 6 cm we find from (1) and (2), $\tau = 3.8\ 10^{-3}$ (independent of distance). The brightness temperature is then:

$$T_b \approx T_e \tau = 38\ \mathrm{K}$$

which will produce a flux density, over a 15″ region, of $S = 120$ mJy. Consequently, its contribution to the total 6 cm flux density of 580 mJy will be small. We conclude that the density obtained in (1) is acceptable and that free-free absorption can explain the low frequency turnover in the spectrum.

We can use the existence of weak polarization at 6 cm to determine more about G70.7 + 1.2 than our earlier conclusion that there must be a non-thermal component. Since only weak polarization is found on the very edge of the shell, it is quite likely that the intrinsic polarization is larger, but that Faraday depolarization has taken place. The degree of depolarization depends upon the rotation measure, which is proportional to $\int n_0 B\, dl$, where B is the line-of-sight magnetic field strength integrated along the path length l. It is clear that l will be shorter along the edge of a sphere than through its centre. Hence the polarization we observe is consistent with the remnant after substantial Faraday depolarization. The fact that practically no polarization is seen along the eastern edge could be the result of depolarization in the H II region seen optically (Fig. 1 and Sect. 3.2), which we have argued lies between us and the radio shell.

Since little polarization is observed at 6 cm, we will assume $\lambda_{1/2}$ (see e.g. Strom, 1973) < 6 cm. Consequently, we have,

$$8.1\ 10^5 \int n_0\, B\, dl > 2/(0.06)^2. \quad (3)$$

The minimum energy in the radio source is calculated to be, $E_m \approx 1.2\ 10^{44}\, d^{17/7}$ erg. The corresponding equipartition magnetic field strength is about $4.5\ 10^{-4}\, d^{-2/7}$ Gauss, and including factors for a random component and geometry, we estimate $B \approx 2\ 10^{-4}\, d^{-2/7}$ Gauss should be used in (3). For $l = 0.07$ pc/kpc we then obtain

$$n_0 > 50\, d^{-5/7}\,\mathrm{cm}^{-3}.$$

This is consistent with our other density estimates.

The total radio luminosity of G70.7 + 1.2 is estimated to be,

$$L_{\mathrm{radio}} \approx 3\ 10^{31}\, d^2\,[\mathrm{kpc}].$$

For a distance of 3 kpc, we obtain a radio luminosity of $3\ 10^{32}$ erg s^{-1}. This is one or two orders of magnitude weaker than typical SNR's, another reason which makes it difficult to interpret G 70.7 + 1.2 as an ordinary supernova remnant.

3.4. Infrared emission from G70.7 + 1.2: a red star and a molecular cloud/H II region system

The infrared data on G70.7 + 1.2 are very different from what is commonly observed in compact H II regions. The LRS spectrum (7.8–23 μm) contains emission features at 7.7 and 11.3 μm, but not the emission lines from photo-ionized gas usually present in compact H II regions. Indeed, all the known compact H II regions which have been detected by the LRS show several gas emission lines such as [Ne II] and [S III] in their infrared spectrum. The 3 μm spectrum of G 70.7 + 1.2 also does not contain the Pf γ line of hydrogen at 3.74 μm which is commonly observed in compact H II regions. The far infrared spectrum is also different from that of H II regions which normally have a flux much larger at 100 μm than at 60 μm. The infrared data thus suggest that their origin is

© European Southern Observatory • Provided by the NASA Astrophysics Data System

1988A&A...193..248J

not in a compact H II region. The near infrared spectrum (3 μm spectrum and near-IR photometry) originates in a compact source which coincides in position with object 1 in Fig. 1a. The LRS spectrum originates in a region centred on object 1 but possibly more extended (≈10″ to 15″) than the optical and near-IR emission. The far-infrared emission seems even more extended (possibly a few arcminutes) and may originate in a molecular cloud, or possibly an extended low excitation H II region.

The high ratios of 60 and 100 μm fluxes to 12 and 25 μm (Table 1) point to the presence of a large amount of cold dust. At a distance of 3 kpc, the total mass of dust in the cloud is estimated to be of the order of $10^{-2}\,M_\odot$ and the total infrared luminosity of the order of $10^4\,L_\odot$.

The near infrared spectrum of G70.7 + 1.2 contains emission bands which are the signature of very small grains or molecules of the Polycyclic Aromatic Hydrocarbons family (Léger and Puget, 1984). These bands are the strong 11.3 μm feature seen in the LRS spectrum (Fig. 4), together with a strong 7.7 μm feature of which only the long wavelength slope appears on the spectrum. There is also a feature at 3.3 μm (Fig. 5) which is significantly brighter in the spectrum obtained with a 26″ beam than with a 12″ beam. This shows that the particles responsible for this emission are not only confined around the central object responsible for the near-IR photometry emission, but are also present at a distance of 0.2 to 0.3 pc from this object. The near infrared photometric data have been measured with a 12″ beam centred at the position of object 1. The magnitudes obtained (Table 1) are typical of a red late-type star. We have compared the LRS spectrum of G70.7 + 1.2 to those of two Wolf-Rayet type nuclei of planetary nebulae bright in the infrared, Hen 1044 and CP − 56°8032, classified as [WC11] (van der Hucht et al., 1981), and we find that they have very similar shapes and spectral features, although G70.7 + 1.2 is much fainter than the other two. This is also true for their 3 μm spectra (Allen et al., 1982); but the spectra of these objects are not so similar at far-infrared wavelengths: the infrared spectra of the two [WC11] stars peak at 25 μm while G70.7 + 1.2 peaks at 60 to 100 μm.

3.5. X-ray data: constraint on the density

The 3σ upper-limit obtained with the LE experiment onboard EXOSAT can be used to derive an upper-limit to the flux in the 0.05–2 keV band. In calculating this upper-limit we make use of the plasma model of Mewe and Gronenschild (1985) which describes the spectral properties of an optically thin plasma in collisional ionization equilibrium. The calculations are carried out for a range of typical values for both the shock temperature T_S, i.e. the temperature of the plasma shocked by the ejected matter, and the hydrogen column density on the line-of-sight N_H. The results are given in Table 6.

Table 6 also gives an upper-limit to the emission normalisation constant C which is defined as:

$$C\,d_{pc}^2 = \int n_e\,n_H\,dV \qquad (4)$$

in which d_{pc} is the distance to the source in pc, n_e, and n_H the electron and the hydrogen number density (in cm^{-3}) of the shocked plasma, respectively. By assuming that the hydrodynamics of the system can be described by a Sedov model, Eq. (4) can be rewritten to give:

$$C = 3.14\ 10^{56}\,n_0^2\,d_{pc}\,\theta_s^3\ cm^{-3}\,pc^{-2}$$

in which n_0 is the number density of the unshocked plasma (in cm^{-3}) and θ_s the angular shock radius of the system (in radian). The Sedov model assumption is thought to be plausible, even in the case of a very young SNR, since simple calculations show that, for a type I supernova in a medium of initial density $n_0 = 100\,cm^{-3}$, the free expansion phase, preceding the Sedov phase, can be as short as 100 years. Adopting a distance of 3 kpc and an angular shock radius of about 8″, we obtain:

$$C \leqq 5\ 10^{46}\,n_0^2\,cm^{-3}\,pc^{-2}.$$

Referring to the results obtained from the optical data (see Sect. 3.2) the value of n_0 is somewhere between 10 and 100 cm^{-3}, in which case we find:

Table 6. Upper limit of X-ray flux as a function of shock temperature

T_S (keV) \ N_H (cm^{-2})	10^{20}	$5\ 10^{20}$	10^{21}	$5\ 10^{21}$	10^{22}
0.1	$C \leqq 4.3\ 10^{47}$	$3.6\ 10^{48}$	$1.1\ 10^{49}$	$5.1\ 10^{50}$	$1.1\ 10^{52}$
	$F \leqq 0.04$	0.33	1.0	48	1021
0.2	$5.3\ 10^{47}$	$1.3\ 10^{48}$	$2.2\ 10^{48}$	$2.0\ 10^{49}$	$1.5\ 10^{50}$
	0.07	0.18	0.30	2.8	20.1
0.5	$7.8\ 10^{47}$	$1.4\ 10^{48}$	$1.9\ 10^{48}$	$8.1\ 10^{48}$	$3.3\ 10^{49}$
	0.12	0.22	0.29	1.3	5.1
1.0	$1.3\ 10^{48}$	$2.9\ 10^{48}$	$4.0\ 10^{48}$	$1.3\ 10^{49}$	$3.2\ 10^{49}$
	0.12	0.26	0.35	1.2	2.9
2.0	$1.7\ 10^{48}$	$3.9\ 10^{48}$	$5.7\ 10^{48}$	$2.0\ 10^{49}$	$4.6\ 10^{49}$
	0.10	0.24	0.35	1.3	2.9
5.0	$2.0\ 10^{48}$	$4.7\ 10^{48}$	$6.8\ 10^{48}$	$2.4\ 10^{49}$	$5.4\ 10^{49}$
	0.11	0.25	0.36	1.3	2.8

Notes:
C is the emission normalisation constant in cm^{-3}/pc^2
F is the source flux in μJy
Numbers are derived by using a 3σ upper-limit of $3.7\ 10^{-4}$ EXOSAT counts per second

© European Southern Observatory • Provided by the NASA Astrophysics Data System

1988A&A...193..248J

$C \leqq 5\ 10^{48}\,\mathrm{cm}^{-3}\,\mathrm{pc}^{-2}$ $(n_0 = 10\,\mathrm{cm}^{-3})$

$C \leqq 5\ 10^{50}\,\mathrm{cm}^{-3}\,\mathrm{pc}^{-2}$ $(n_0 = 100\,\mathrm{cm}^{-3})$.

A comparison between these upper-limits on C and those given in Table 6 indicates that an upper-limit on the density n_0 of about $100\,\mathrm{cm}^{-3}$ is quite reasonable within the range of shock temperatures and column densities considered. A higher pre-shock density n_0 should lead to a statistically significant X-ray detection of the source.

4. Possible scenarios for the nature of G70.7 + 1.2

A plausible interpretation of G70.7 + 1.2 is a compact supernova shell in a high density region which includes H II emission, some of which absorbs the non-thermal radio emission at low frequencies. As detailed above, we believe this can explain the radio spectrum, polarization and shell morphology, the optical spectrum which has all the hallmarks of shock excitation, and the infrared emission features. There is as yet no direct radio evidence for thermal emission, but we have pointed out that it could be so weak as to have yet escaped detection. This is clearly an area where additional observational work is required. The nature of the compact near-infrared source has also yet to be clarified. It may not be directly related to the non-thermal shell, however.

The modest size of the shell (0.21 pc at $d = 3$ kpc) when compared with that of young supernova remnants which are at least 10 times larger, suggests a young remnant, or one in which the energy released was unusually low. There are, however, several possible objections to such an interpretation. One is the amount of energy calculated above, which is considerably smaller than that found for young shell remnants in the radio. This objection can be countered by noting that the onset of radio emission (after an initial outburst associated with the supernova itself) is not immediate. One can argue that we are seeing a supernova remnant in the process of turning on.

Another realistic objection against a young supernova remnant is the lack of evidence for high velocity gas in the optical spectra. While the spectra may show shifts consistent with velocities of a few hundreds $\mathrm{km\,s}^{-1}$, there is clearly no sign of gas moving at $1000\,\mathrm{km\,s}^{-1}$ or more, or the equivalent line broadening (the former is seen in Cas A, the latter in Tycho). However, here again the evidence is not conclusive. Observationally, we can note both that high velocities have yet to be observed in Kepler (they are not present in the most prominent nebulosity), and that supernovae have been observed with quite small initial velocities (Zwicky's Type V class, for example). Moreover, a shock moving into ambient gas of much higher density will have a velocity smaller by the square root of the density contrast. If the region surrounding G70.7 + 1.2 is 100 times denser than the interior of the shell, then shock velocities of 1000's of $\mathrm{km\,s}^{-1}$ will be transformed into 100's of $\mathrm{km\,s}^{-1}$.

A third objection to a young remnant has been raised by Green (1986): if it is relatively close, why was its parent supernova not seen? Here again, the case is not clearcut. For a Type II or Type Ib supernova, we might expect $M_v = -18$. At 3 kpc and assuming extinction of 1^{m}/kpc, this would give $m_v = -2.5$ at maximum. Such a star is readily observable, but could also easily have been missed if maximum occurred during winter when this area of the sky is not visible. Moreover, Type II maxima are quite variable, so an even fainter m_v cannot be ruled out.

The optical image, the weakness of the radio luminosity, the absence of X-ray emission, and the presence of an object with a red continuum and lots of optical emission lines make G70.7 + 1.2 quite different from most well-known supernova remnants. In fact, to account for its radio luminosity, there is no need for such a violent event as a supernova explosion. The conversion efficiency of kinetic energy into radio emission is of the order of a few percent (Pelletier and Roland, 1986). To produce a radio luminosity of 10^{32} to $10^{33}\,\mathrm{erg\,s}^{-1}$, we need only a kinetic energy input of 10^{34} to $10^{35}\,\mathrm{erg\,s}^{-1}$. This can be produced by a stellar superwind occurring in the termination of the AGB phase of a red giant or supergiant, as described by Iben and Renzini (1983). This last phase is very short ($\approx 10^3$ yr) compared to the previous AGB lifetime (10^5 to 10^6 yr) during which the normal wind dominates (i.e. $dM/dt = -4\ 10^{-13}\,\eta\,L/gR$, with L = luminosity, g = surface gravity, R = radius in solar units, and $1/3 < \eta < 3$, Reimers, 1975). In this picture, low and intermediate mass stars ascend the AGB losing mass according to the above rate, and when a critical luminosity is reached most of the residual H-rich envelope is ejected on a very short timescale thus generating a superwind with average MLR's ranging from 10^{-5} to $10^{-3}\,M_\odot\ \mathrm{yr}^{-1}$, at velocities which can reach a few 10's of $\mathrm{km\,s}^{-1}$, thus driving a shock wave into the surrounding dense interstellar matter. The kinetic energy input provided by such a superwind will range from 10^{33} to $10^{35}\,\mathrm{erg\,s}^{-1}$. This is enough to account for a radio luminosity of 10^{32} to $10^{33}\,\mathrm{erg\,s}^{-1}$. The energy provided by a supernova would be much higher and therefore the radio emission should be much higher. Radio luminosities of other well-known SNR's are of the order of 10^{34}–$10^{35}\,\mathrm{erg\,s}^{-1}$. It seems plausible that there is in G70.7 + 1.2 a supergiant undergoing violent outbursts. The red continuum suggests a red supergiant ($M < 60\,M_\odot$), while the iron emission lines suggest a luminous blue supergiant ($M > 60\,M_\odot$). With all the dust present in the area, it is also possible that a blue star is seen strongly reddened.

Finally, a third possibility for the nature of G70.7 + 1.2 is that it could be the remnant of a nova. Reynolds and Chevalier (1984) have shown that the shock or turbulent processes that act in supernova remnants ($E_0 \approx 10^{51}$ erg) also act in the similar but far less energetic nova outbursts ($E_0 \approx 10^{45}$ erg). In their example of nova GK Persei 1901, several aspects are quite similar to G70.7 + 1.2. These are: a radio shell morphology with a star (GK Persei itself) located inside the shell but not centred on the radio peak, very weak polarization at 6 cm, a spectral index of 0.67 between 4835 and 1465 MHz, a kinetic energy input of $\sim 10^{45}$ ergs, corresponding to a luminosity of $\sim 10^{35}\,\mathrm{erg\,s}^{-1}$, and a radio luminosity being 2 or 3 orders of magnitude weaker.

5. Summary and conclusion

The observational data presented in this paper throw more light on the nature of the rather peculiar source G70.7 + 1.2:

i) The radio 20 and 6 cm maps show a shell structure, $\sim 20''$ in diameter, with a radio spectral index of ~ 0.6 at high frequencies ($\nu > 1$ GHz), which is commonly observed for several well-known supernova remnants.

ii) The optical spectra along two perpendicular scans (N–S and E–W) across the region clearly show the existence of shock excited gas ($\sim 16''$ in extent), and an adjacent H II region extending east and north, over a distance of at least $15''$ in both directions.

iii) The optical spectra show the presence of a continuum point source coinciding with a very strong peak of Hα emission and the emission of numerous optical lines, most of them due to iron and a few possibly to nitrogen.

© European Southern Observatory • Provided by the NASA Astrophysics Data System

1988A&A...193..248J

iv) The infrared emission accounts for at least two components: the far-infrared emission is due to an extended molecular cloud – H II region system; the near-infrared continuum and emission features come from the immediate surrounding of the optical continuum source and show the presence of Polycyclic Aromatic Hydrocarbon molecules.

v) The diagnostic criterion, for the identification of supernova remnants, of strong [S II] lines relative to Hα coinciding with radio emission is a necessary but not sufficient condition. Some galactic objects, identified as SNR's on the basis of this criterion, may have been misclassified.

vi) In the light of these new observations, it seems that G 70.7 + 1.2 is an object undergoing events not as violent as in classical SNR's but much more unusual than just an H II region. It could be:

– A very young compact supernova remnant, expanding in a high density medium which absorbs part of the non-thermal radiation.

– A supergiant violently ejecting its last layer of circumstellar matter into a molecular cloud.

– The remnant of a nova.

Future observations are necessary to discriminate among the various scenarios.

Acknowledgements. We thank the Director of the Royal Greenwich Observatory for having allocated time during a Director's night on the INT in order to obtain the optical spectra, and A. Pickles (Groningen and RGO) who actually made this observation. We are very grateful to J. Roland, V. Icke and K.A. van der Hucht for useful discussions. We thank H.J. Habing for his support of this work and F.P. Israel for his suggestions in its early phases. We are also very grateful to G.F.R.N. Rhee, M.H.K. de Grijp, G.M. Stirpe, H. Greidanus, F. Sloff and G. Duvert for their help and introduction to using various software packages. We thank J. Bally for having shown us some CO data prior to publication. We thank the staff at UKIRT and at the EXOSAT Observatory for their help during the infrared and X-ray observations respectively.

The NRAO which runs the VLA is operated by Associated Universities Inc., under contract with the U.S. National Science Foundation. The WSRT is operated by the Netherlands Foundation for Radio Astronomy with the financial support of the Netherlands Organisation for the advancement of pure research (ZWO). The Laboratory for Space Research is supported financially by ZWO. MJAO acknowledges ASTRON/ZWO for financial support (grant 782-373-009). The Infrared Astronomical Satellite was developed and operated by the Netherlands Agency for Aerospace Programs (NIVR), the U.S. National Aeronautics and Space Administration (NASA) and the U.K. Science and Engineering Research Council (SERC).

References

Allen, D.A., Baines, D.W.T., Blades, J.C. Whittet, D.C.B.: 1982, *Monthly Notices Roy. Astron. Soc.* **199**, 1017

Baars, J.W.M., Genzel, R., Pauliny-Toth, I.I.K., Witzel, A.: 1977, *Astron. Astrophys.* **61**, 99

Blair, W.P., Kirshner, R.P.: 1985, *Astrophys. J.* **289**, 582

Brouw, W.N.: 1971, PhD thesis, University of Leiden

Chiosi, C., Maeder, A.: 1986, *Ann. Rev. Astron. Astrophys.* **24**, 329

Colla, G., Fanti, C., Fanti, R., Ficarra, A., Formiggini, L., Gandolfi, E., Grueff, G., Lari, C., Padrielli, L., Roffi, G., Tomasi, P., Vigotti, M.: 1970, *Astron. Astrophys. Suppl. Ser.* **1**, 281

Clark, B.G.: 1980, *Astron. Astrophys.* **89**, 377

Danziger, I.J., Murdin, P.G., Clark, D.H., d'Odorico, S.: 1979, *Astron. Astrophys.* **186**, 555

Dennefeld, M., Kunth, D.: 1981, *Astron. J.* **86**, 989

Fesen, R.A., Blair, W.P., Kirshner, R.P.: 1985, *Astrophys. J.* **292**, 29

Gratton, L.: 1963, in *Star Evolution*, Proceedings of the International School of Physics Enrico Fermi, Course 28, ed. Gratton, Academic Press, New-York, p. 297

Green, D.A.: 1985, *Monthly Notices Roy. Astron. Soc.* **216**, 691

Green, D.A.: 1986, *Monthly Notices Roy. Astron. Soc.* **219**, 39P

Helfand, D.J., Becker, R.H.: 1984, *Nature* **307**, 215

Högbom, J.A.: 1974, *Astron. Astrophys. Suppl.* **15**, 417

Hucht, K.A. van der, Conti, P.S., Lundström, I., Stenholm, B.: 1981, *Space Sci. Rev.* **28**, 227

Iben, I., Jr., Renzini, A.: 1983, *Ann. Rev. Astron. Astrophys.* **21**, 271

Israel, F.P.: 1976, *Astron. Astrophys.* **48**, 193

Kriss, G.A., Becker, R.H., Helfand, D.J., Canizares, C.R.: 1985, *Astrophys. J.* **288**, 703

Léger, A., Puget, J.-L.: 1984, *Astron. Astrophys.* **137**, L5

Longmore, A.J., Clark, D.H., Murdin, P.: 1977, *Monthly Notices Roy. Astron. Soc.* **181**, 541

Mathewson, D.S., Clarke, J.N.: 1973, *Astrophys. J.* **180**, 725

Mendoza, C., Zeippen, C.J.: 1982, *Monthly Notices Roy. Astron. Soc.* **198**, 127

Mewe, R., Gronenschild, E.H.E.M., 1985, *Astron. Astrophys. Suppl. Ser.* **62**, 197

Minkowski, R.: 1948, *Pub. Astron. Soc. Pacific.* **60**, 386

Muizon, M. de, Habing, H.J.: 1985, in *Nearby molecular clouds*, Proc. 8th IAU European Regional Astronomy Meeting, ed. G. Serra, Lect. Notes Phys. **237**, 130

Noordam, J.E., de Bruyn, A.G.: 1982, *Nature* **299**, 597

Pelletier, G., Roland, J.: 1986, *Astron. Astrophys.* **163**, 9

Pradhan, A.K.: 1978, *Monthly Notices Roy. Astron. Soc.* **183**, 89 P

Raymond, J.C.: 1984, *Ann. Rev. Astron. Astrophys.* **22**, 75

Read, P.L.: 1981, *Monthly Notices Roy. Astron. Soc.* **195**, 371

Reich, W., Fürst, E., Althenhoff, W.J., Reich, P., Junkes, N.: 1985, *Astron. Astrophys.* **151**, L 10

Reich, W., Fürst, E., Stuffen, P., Reif, K., Haslam, C.G.T.: 1984, *Astron. Astrophys. Suppl. Ser.* **58**, 197

Reimers, D.: 1975, in *Problems in Stellar Atmospheres and Envelopes*, eds. B. Baschek, W.H. Kegel, G. Traving, Springer, Berlin, Heidelberg, New York, p. 229

Reynolds, S.P., Chevalier, R.A.: 1984, *Astrophys. J. Letters* **281**, L 33

Scheuer, P.A.G., Williams, P.J.S.: 1968, *Ann. Rev. Astron. Astrophys.* **6**, 321

Stahl, O., Wolf, B., de Groot, M., Leitherer, C.: 1985, *Astron. Astrophys. Suppl. Ser.* **61**, 237

Stasińska, G.: 1982, *Astron. Astrophys. Suppl. Ser.* **48**, 299

Strom, R.G.: 1973, *Astron. Astrophys.* **25**, 303

Shull, J.M., McKee, C.F.: 1979, *Astrophys. J.* **227**, 131

Thackeray, A.D.: 1967, *Monthly Notices Roy. Astron. Soc.* **135**, 51

Thackeray, A.D.: 1977, *Memoirs Roy. Astron. Soc.* **83**, 1

Vreux, J.M., Dennefeld, M., Andrillat, Y.: 1983, *Astron. Astrophys. Suppl. Ser.* **54**, 437

© European Southern Observatory • Provided by the NASA Astrophysics Data System